

Non-Hermitian interferometer: Unidirectional amplification without distortion

C. Li, L. Jin and Z. Song*

School of Physics, Nankai University, Tianjin 300071, China

A non-Hermitian interferometer can realize asymmetric transmission in the presence of imaginary potential and magnetic flux. Here, we propose a non-Hermitian dimer with an unequal hopping rate by an interferometer-like cluster in the framework of tight-binding model. The intriguing features of this design are the wave-vector independence and unidirectionality of scattering, which amplifies wavepacket without distortion and absorbs incoherent wave without reflection. The absorption relates to the system spectral singularities, the dynamical behaviors of the spectral singularities are also investigated analytically and numerically.

PACS numbers: 03.65.Nk, 05.60.Gg, 11.30.Er, 42.25.Bs

I. INTRODUCTION

Nowadays a non-Hermitian quantum mechanics has emerged as a versatile platform for exploring the difficulties for fabricating functional devices in Hermitian regime. The main mechanism is based on the existence of imaginary potential which has been investigated theoretically [1–12] and realized in experiment [13–22] as an ideal building block of non-Hermitian system. However, it has been shown a pure complex potential cannot realize asymmetric transmission [23–25], which is the central goal in many works [26–28]. On the other hand, another ideal building block possessing asymmetric transmission is a asymmetric dimer, which has an unequal hopping strength in the framework of tight-binding model.

In this paper, we investigate the possible mechanism of asymmetric transmission in a non-Hermitian system. We show that a non-Hermitian interferometer can realize asymmetric transmission due to the combination of imaginary potential and magnetic flux. As a demonstration, we construct a non-Hermitian dimer with an unequal hopping rate by an interferometer-like cluster in the framework of tight-binding model. The intriguing feature of this design are the wave-vector independent and unidirectional scattering, which allows the reflectionless amplified transmission of wavepacket without any distortion. With optimal system parameters, it acts as an absorber for both coherent and incoherent incident waves. Some dynamical behaviors related to the spectral singularities are also presented analytically and numerically.

This paper is organized as follows. In Section II, we depict the physical mechanism of asymmetric transmission arising from the combination of imaginary potential and magnetic flux. In Section III, we present a interferometer-like scattering center, which is shown to be equivalent to an asymmetric dimer. In Section IV we study the transmission feature of this design. In Section V, the spectral singularity of the Hamiltonian is examined. Finally, we give a summary in Section VII.

II. ASYMMETRIC TRANSMISSION

It is well known that a Hermitian scattering center possesses the feature of symmetric transmission, i.e., the transmission and reflection coefficients are independent of the input direction of an incident wave. It is true for the case with a threading magnetic flux, which may break the time reversal symmetry. On the other hand, it has been shown that, a non-Hermitian scattering center but with the time reversal symmetry still has symmetric transmission [25]. A typical scattering center of such kind is a Hermitian system with additional imaginary potentials. It has been found that the magnetic flux in a non-Hermitian scattering center may lead to asymmetric transmission. The mechanism of this behavior can be understood by the following simple example.

We start with a simplest non-Hermitian scattering center, an on-site imaginary potential embedded in the center of an infinite chain with the Hamiltonian

$$H_\gamma = H_{\text{lead}} + H_c \quad (1)$$

where

$$H_{\text{lead}} = - \sum_{j=1}^{\infty} (|j\rangle \langle j+1| + |-j\rangle \langle -j-1| + \text{H.c.}), \quad (2)$$

is the Hamiltonian of two leads and the scattering center Hamiltonian

$$H_c = -(|-1\rangle + |1\rangle) \langle 0| + \text{H.c.} + i\gamma |0\rangle \langle 0|. \quad (3)$$

The Bethe Ansatz solution [29] gives the transmission and reflection coefficients

$$T_k(\gamma) = \frac{4 \sin^2 k}{(2 \sin k - \gamma)^2}, \quad R_k(\gamma) = \frac{\gamma^2}{(2 \sin k - \gamma)^2}, \quad (4)$$

for the incident wave from left or right side. We note that T_k is γ - and k -dependent but independent of incident direction. Two typical cases are of $\gamma = -2$ and 2 for $k = \pi/2$, with two different features, i.e.,

$$T_{\pi/2}(2) = \infty, \quad T_{\pi/2}(-2) = 1/4. \quad (5)$$

* songtc@nankai.edu.cn

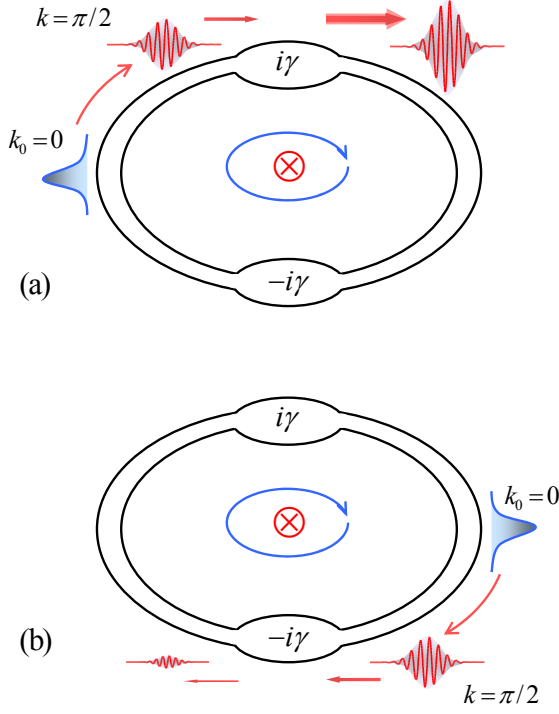


FIG. 1. (Color online) Schematic illustration of a simple non-Hermitian configuration to demonstrate the effect of imaginary potential and magnetic flux on the dynamics of a wavepacket. It is a non-Hermitian ring with the non-Hermiticity arising from the imaginary potentials. The magnetic flux breaks left-right symmetry. Initially, a stationary wavepacket (blue) with vector $k_0 = 0$ is located at the left (a) or right (b) respectively. In both cases, the central momentum of the wavepacket can be shifted to $\pi/2$ by a well-prepared flux. It makes two wavepackets face two different situations. (a) The wavepacket moves up and encounters the potential $2i$. It acquires an infinite transmission. (b) The wavepacket moves down and is scattered by the potential $-2i$ and gets a finite transmission.

On the other hand, as a Hermitian quantity, the magnetic flux has two features: i) it can shift the wave vector of a plane wave; ii) it usually breaks the symmetry in real space. Combining the effects of imaginary potential and flux, the asymmetric transmission can be realized in principle. To demonstrate this point, we consider a concrete system, a non-Hermitian ring, which is schematically illustrated in Fig. 1. The non-Hermiticity of the system arises from the imaginary potentials. The magnetic flux breaks left-right symmetry. In the following we examine the effects of potential and flux on the dynamics of a wavepacket. Consider a stationary wavepacket with vector $k_0 = 0$, which is initially located at the left or right, respectively. In both cases, the central momentum of the wavepacket can be shifted to $\pi/2$ by a well-prepared flux [30]. It makes two wavepackets face two different situations. For the left one, it is scattered by

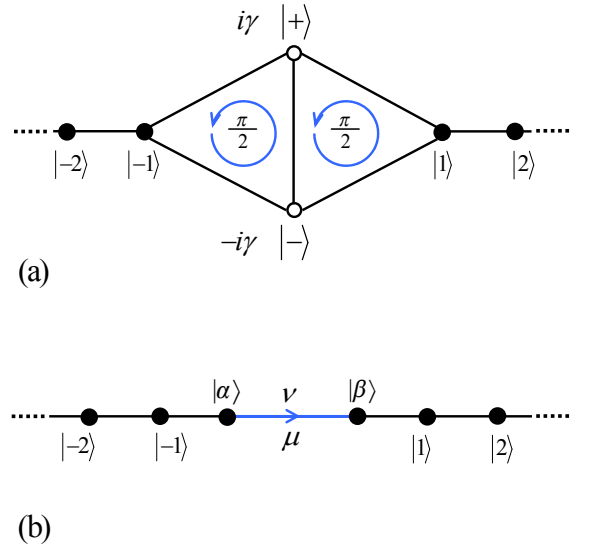


FIG. 2. (Color online) Sketch of the system considered in this work and schematic illustration of the equivalent Hamiltonian with asymmetric transmission. The black bonds denote Hermitian hopping, while the blue arrowed bond denotes the hopping with asymmetric amplitudes. (a) The non-Hermitian scattering center embedded in a discrete waveguide. It consists of Hermitian hopping, magnetic flux, and imaginary potentials. The coexistence of flux and imaginary potentials breaks the symmetry of transmission. (b) The equivalent system of (a), in which the scattering center is simply an asymmetric dimer with unequal hopping strength (μ, ν) .

the potential $2i$ and get an infinite transmission, while the right one is scattered by the potential $-2i$ and gets a finite transmission. Apparently, it is due to the left-right symmetry breaking induced by the flux. The imaginary potential takes an important role. If we replace $i\gamma$ by real number V , we have the corresponding transmission coefficient $T_k(V) = 4 \sin^2 k / (4 \sin^2 k + V^2)$, which is independent of the sign of V (see Appendix a). It accords with the exact result for a Hermitian scattering center with flux [25]. On the other hand, imaginary potentials cannot lead to asymmetric transmission solely, since the system is left-right symmetric in the absence of flux.

So far we have given a semi-quantitative analysis about the realization of asymmetric transmission. For a tight-binding lattice network, the equivalence between the imaginary potential and the input (output) lead is proposed [31–33]. In the following section, we will construct a simple but efficient system, which will be shown to be equivalent to an asymmetric dimer, to demonstrate the novel feature of non-Hermitian system.

III. ASYMMETRIC DIMER

In this section, we will present a concrete scattering center, which is exactly solvable and deliberately constructed to exhibit unambiguous asymmetric transmis-

sion. This study is of significant not only for the non-Hermitian quantum mechanics but also for applications in quantum technology. Now the model we study becomes

$$H = H_{\text{lead}} + H_{\text{int}}. \quad (6)$$

The concerned scattering center is a non-Hermitian Aharonov-Bohm interferometer, with the Hamiltonian

$$H_{\text{int}} = -\frac{1}{\sqrt{2}} \sum_{\sigma=\pm} (e^{-i\sigma\phi} |-1\rangle + e^{i\sigma\phi} |1\rangle) \langle\sigma| + \delta |+\rangle \langle -| + \text{H.c.} + i\gamma \sum_{\sigma=\pm} \sigma |\sigma\rangle \langle\sigma|, \quad (7)$$

where parameters δ and γ are real numbers and $\phi = \pi/4$. It is constructed by a Hermitian cluster with additional imaginary potentials. The geometry of the cluster and the process of simplification are illustrated in Fig. 2. Recently, the transmission problem for similar non-Hermitian Aharonov-Bohm 4-site rings is studied in [33, 34].

A tight-binding network is constructed topologically by the sites and various connections between them. There are three types of basic non-Hermitian clusters leading to the non-Hermiticity of a discrete non-Hermitian system: i) complex on-site potential denoted as $e^{i\varphi} |l\rangle \langle l|$; ii) non-Hermitian dimer denoted as $e^{i\varphi} (|l\rangle \langle j| + \text{H.c.})$, where φ is real; iii) asymmetric hopping amplitude dimer denoted as $\mu |l\rangle \langle j| + \nu |j\rangle \langle l|$ with asymmetric parameters $\mu \neq \nu$ being real numbers, which has been used in modeling a delocalization phenomenon relevant for the vortex pinning in superconductors [35]. The former two types of non-Hermitian clusters violate \mathcal{T} symmetry, while the last one does not. The non-Hermiticity of the present system only arises from the imaginary potentials. In previous work, it has been shown by an example that, the first and second types of clusters are transformable with each other [33]. In the following, we will show that our model can be reduced to the third types of dimers by a simplification process.

By taking the linear transformation

$$\begin{cases} |\alpha\rangle = \frac{1}{\sqrt{2}} (e^{i\pi/4} |+\rangle + e^{-i\pi/4} |-\rangle), \\ |\beta\rangle = \frac{i}{\sqrt{2}} (e^{i\pi/4} |+\rangle - e^{-i\pi/4} |-\rangle), \end{cases} \quad (8)$$

the Hamiltonian of the scattering center is reduced to

$$H_{\text{int}} = -(|-1\rangle \langle\alpha| + |1\rangle \langle\beta|) + \text{H.c.} + (\delta + \gamma) |\alpha\rangle \langle\beta| + (\delta - \gamma) |\beta\rangle \langle\alpha|, \quad (9)$$

which is schematically illustrated in Fig. 2(b). This let us can rewrite the whole Hamiltonian as an equivalent one

$$H_{\text{eq}} = -\sum_{j=1}^{\infty} (|j\rangle \langle j+1| + |-j\rangle \langle -j-1|) - (|-1\rangle \langle\alpha| + |1\rangle \langle\beta|) + \text{H.c.} - \mu |\alpha\rangle \langle\beta| - \nu |\beta\rangle \langle\alpha|, \quad (10)$$

for scattering problem. Here parameters

$$\mu = -(\delta + \gamma), \quad \nu = -(\delta - \gamma) \quad (11)$$

are asymmetric hopping amplitudes, exhibiting the feature of asymmetric transmission in a simple way. In the following sections, we will explore the features of the asymmetric dimer, which can be applied to the original system in Eq. (7).

For an incident plane wave with momentum k incoming from the left with energy $E_k = -(e^{ik} + e^{-ik})$, the scattering wave function $|\psi_k\rangle$ can be obtained by the Bethe Ansatz method. The wave function has the form

$$|\psi_k\rangle = \sum_{j=1}^{\infty} [f^k(j) |j\rangle + f^k(-j) |-j\rangle] + f^k(\alpha) |\alpha\rangle + f^k(\beta) |\beta\rangle \quad (12)$$

where the scattering wave function $f^k(j)$ is in the form of

$$f^k(j) = \begin{cases} e^{ikj} + r_k e^{-ikj}, & j \leq -1 \\ t_k e^{ik(j+1)}, & j \geq 1 \\ 1 + r_k, & j = \alpha \\ t_k e^{ik}, & j = \beta \end{cases}. \quad (13)$$

Here r_k and t_k are the reflection and transmission amplitudes of the incident wave with momentum k , which can be used to identify the spectral singularity of the system. By solving the Schrödinger equation $H |\psi_k\rangle = E_k |\psi_k\rangle$, we obtain

$$r_k = \frac{1 - \mu\nu}{\mu\nu - e^{-i2k}}, \quad t_k = \frac{\nu(1 - e^{-i2k})}{\mu\nu - e^{-i2k}}. \quad (14)$$

Similarly, the solution for an incident wave from right can be obtained by replacing ν with μ .

IV. REFLECTIONLESS AMPLIFICATION

Besides the above property, Eq. (14) also indicate the relation

$$r_k = 0, \quad t_k = \mu, \quad (15)$$

for left incident wave, or

$$r_k = 0, \quad t_k = \nu, \quad (16)$$

for right incident wave when the resonant condition $\mu\nu = 1$ is satisfied. The action of a resonant asymmetric dimer is reflectionless amplified transmission. We note that this amplification is k -independent, which results in deformation free for arbitrary signal.

This feature can be understood by the Eq. (31). We are interested in the case of $\mu\nu = 1$. One can rewrite the

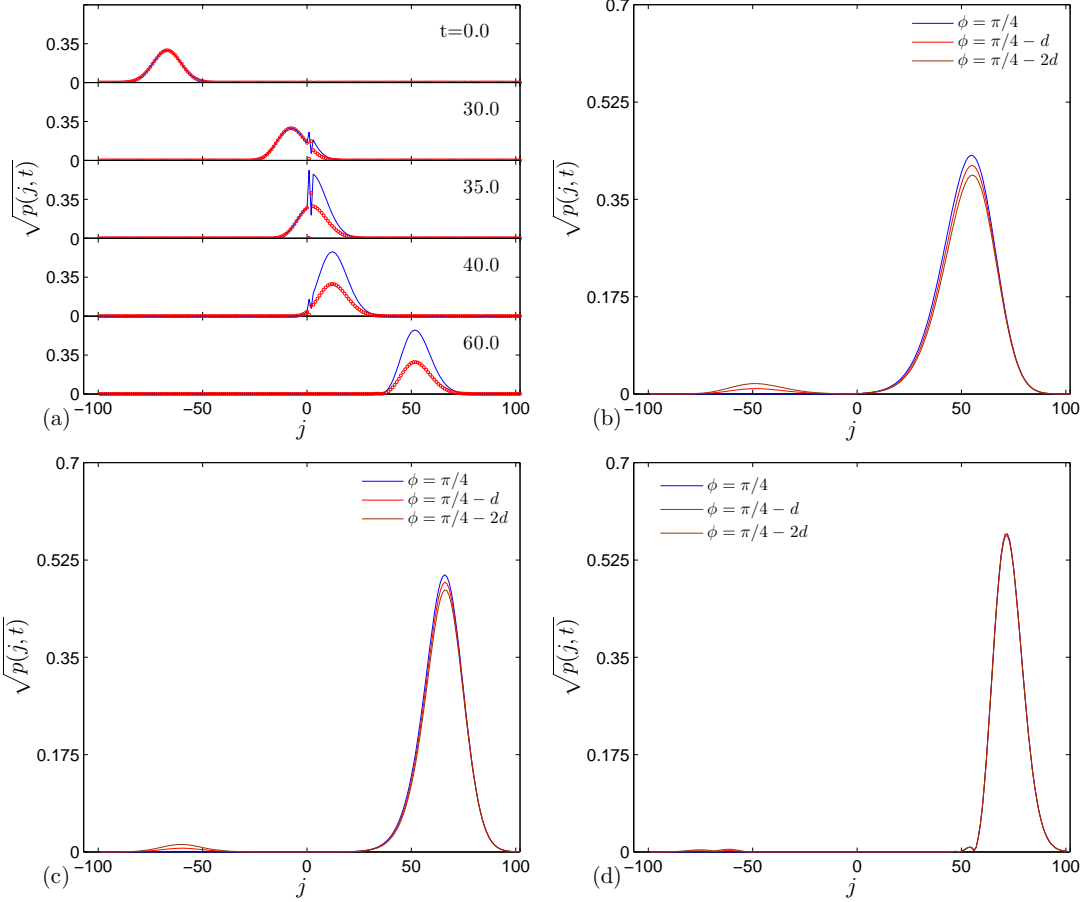


FIG. 3. (color online) The profiles of Dirac norm for time evolution of initial Gaussian wave packets with $w = 0.15$ and several typical k_0 under the systems with parameters $\delta = -1.25$ and $\gamma = 0.75$ but different fluxes. (a) $k_0 = \pi/2$ and $\phi = \pi/4$. The blue line represents the time evolution at several typical instants. As a comparison, the red circle shows the time evolution of the same initial state under the system with parameters $\delta = -1$ and $\gamma = 0$, which corresponds to a uniform chain. It shows a perfect reflectionless amplification with $\nu = 2$. Figs. (b, c, d) show the time evolution at instant $t = 70$ for different initial states with (b) $k_0 = \pi/3$, (c) $k_0 = \pi/2.5$, and (d) $k_0 = \pi/2$, respectively. Here ϕ are deviated from $\pi/4$ in unit of $d = \pi/100$. It shows that this amplifier is immune of the deviation of ϕ for the signal around $k_0 = \pi/2$.

Hamiltonian h_{eq} as

$$h_{\text{eq}} = - \sum_{j=1}^{\infty} \left(\overline{|j\rangle\langle j+1|} + \overline{|j+1\rangle\langle j|} + \overline{|-j\rangle\langle -j-1|} + \overline{|-j-1\rangle\langle -j|} - \overline{|-1\rangle\langle \alpha|} + \overline{|\alpha\rangle\langle -1|} + \overline{|1\rangle\langle \beta|} + \overline{|\beta\rangle\langle 1|} - \overline{|\alpha\rangle\langle \beta|} - \overline{|\beta\rangle\langle \alpha|} \right), \quad (17)$$

which is equivalent to a Hermitian uniform chain. It accords with the fact of $r_k = 0$. When we concern about the Dirac probability, we can take the mapping $\overline{|j\rangle} \rightarrow \sqrt{\frac{\nu}{\mu}} |j\rangle = \nu |j\rangle$, within the right half region.

It indicates that the cluster in Eq. (7) can act as a quantum amplifier under the condition

$$\mu\nu = \delta^2 - \gamma^2 = 1. \quad (18)$$

We introduce the amplification coefficient \mathcal{A} to characterize this phenomenon for an incident plane wave $|k, \text{in}\rangle$

and output plane wave $|k, \text{out}\rangle$, where

$$\mathcal{A}(k) = \frac{\langle k, \text{out} | k, \text{out} \rangle}{\langle k, \text{in} | k, \text{in} \rangle}. \quad (19)$$

A remarkable feature of this design is that

$$\mathcal{A}(k) = \nu^2, \quad \frac{\partial \mathcal{A}(k)}{\partial k} = 0, \quad (20)$$

i.e., the amplification coefficient is k -independent, which leads to the fact that it cannot induce any distortion of a given signal. To demonstrate this point, we perform numerical simulations for the scattering center in Eq. (7). The profiles of evolved states, i.e., $p(j, t) = |\langle j | \varphi(t) \rangle|^2$, which is the probability of the evolved state $|\varphi(t)\rangle$ on the site j , are plotted in Fig. 3(a), which shows that the wave packet $|\varphi(0)\rangle = |\phi(N_A, \pi/2)\rangle$ almost totally passes through the scattering center and the transmitted wave packet is amplified by ν times of the incident amplitude without any signal distortion. Where the initial

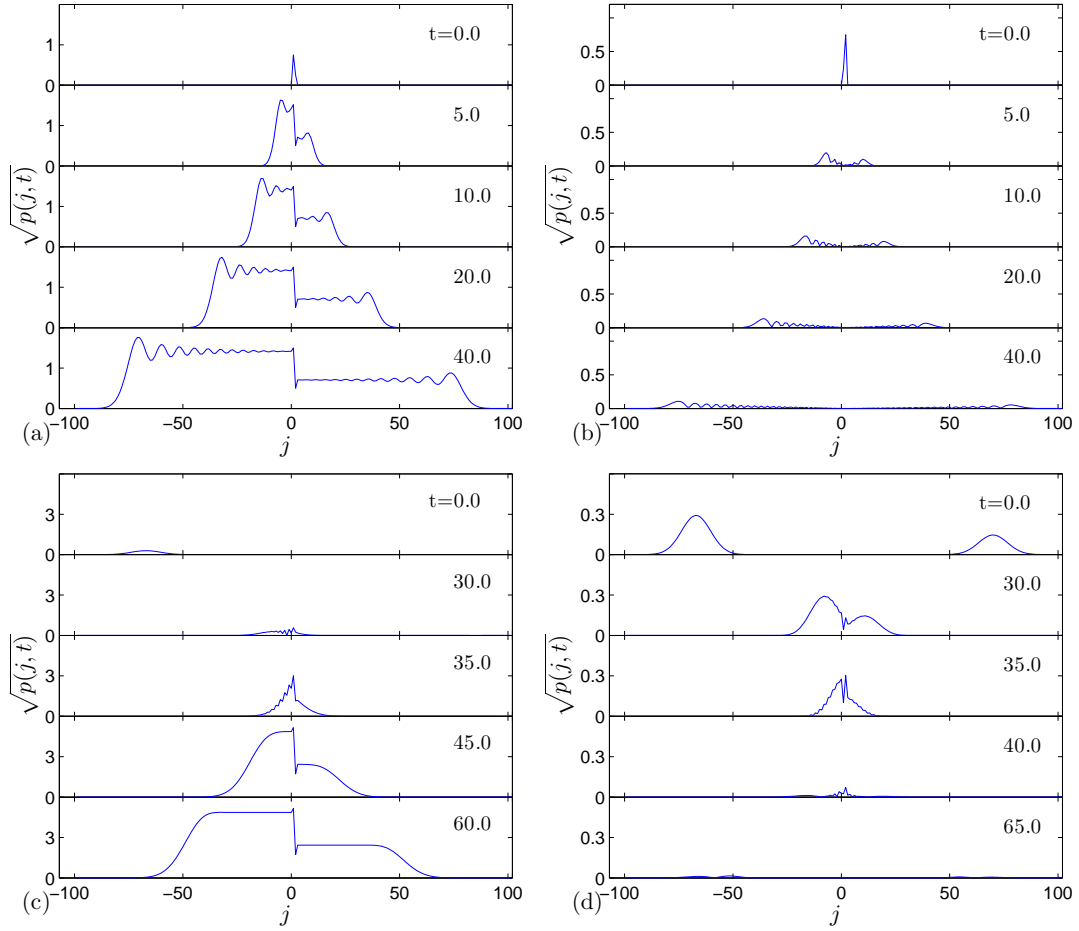


FIG. 4. (color online) The profiles of Dirac norm for evolved states of four types of initial states: (a) The state defined by $|\alpha\rangle + i\nu|\beta\rangle$; (b) The state defined by $|\alpha\rangle - i\nu|\beta\rangle$; (c) A Gaussian wave packet with $w = 0.15$ and $k_0 = \pi/2$; (d) The state defined by Eq. (27) with $w = 0.15$ and $k_0 = \pi/2$. The time evolutions is governed by the Hamiltonian with $\delta = 0.75$ and $\gamma = 1.25$ for all figures, which correspond to $\mu = -2.0$ and $\nu = 0.5$, satisfying the spectral singularity condition $\mu\nu = -1.0$.

state $|\phi(N_A, k_0)\rangle = \Omega_0^{-1/2} \sum_j e^{-\frac{\lambda^2}{2}(j-N_A)^2} e^{ik_0 j} |j\rangle$ represents a Gaussian wave packet with central momentum k_0 and position N_A , $\Omega_0 = \sum_j e^{-\lambda^2(j-N_A)^2}$ is the normalization factor, and the half-width of the wave packet $w = 2\sqrt{\ln 2}/\lambda$ characterizes the size of the local state.

For the experimental realization of quantum amplifier of this design, the deviation of a magnetic flux from the optimal magnitude may change the Eq. (20) in practice. Figs. 3(b,c,d) is the plots of the profiles of evolved Gaussian wave packets under the system with the deviated flux, which are obtained by numerical simulations for Gaussian wave packets with several typical values of central momenta k_0 . It indicates that the deviation of the flux results in the distortion of the shape. One can find that the more ϕ and k_0 deviate from $\pi/4$ and $\pi/2$, respectively, the more distorted signal is obtained from the amplifier. It shows that the quantum amplifier of this design is robust with respect to the deviation of flux.

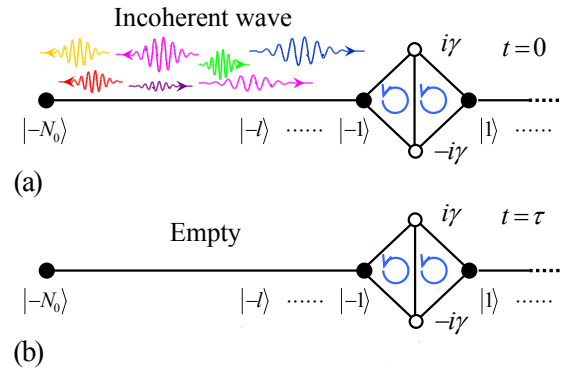


FIG. 5. (Color online) Schematic illustration of a non-Hermitian configuration to demonstrate the perfect absorption for incoherent state. It is the same system as Fig. 2(a) with open boundary condition at left side. (a) Initially, a mixed state is located in the region $[-N_0, -1]$. (b) The incoherent perfect absorption is achieved if the total Dirac probability in the whole system vanishes at relaxation time τ .

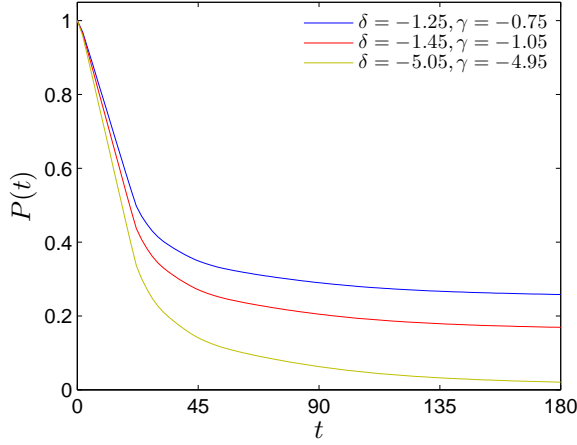


FIG. 6. (Color online) The plots of $P(t)$ for the initial state in Eq. (37), obtained from the time evolution under the configuration illustrated in Fig. 5 with $N_0 = 20$. The inset parameters (δ, γ) corresponds to $\nu = 0.5, 0.4$, and 0.1 , respectively.

V. SPECTRAL SINGULARITY

Recently, the concept of spectral singularity of a non-Hermitian system has gained a lot of attention [36–46], motivated by the possible physical relevance of this since the pioneer work of Mostafazadeh [47]. The majority of previous works do not include the non-Hermitian system with asymmetric dimer. According to Eq. (14), The divergence of r_k and t_k indicates the existence of spectral singularity, which has been pointed out in Ref. [48]. We note that it occurs only at the point $\mu\nu = -1$ for states with $k = \pm\pi/2$. The corresponding wave functions are

$$f^{\pm\pi/2}(j) = \begin{cases} e^{i(\pm\pi/2)j}, & j \leq -1 \\ \nu e^{i(\mp\pi/2)(j+1)}, & j \geq 1 \\ 1, & j = \alpha \\ \nu e^{i(\mp\pi/2)}, & j = \beta \end{cases}. \quad (21)$$

The physics of two states are clear, representing complete absorption and self-sustained emission of two opposite waves. The intriguing feature of the spectral singularity is the coexistence of two states. It indicates that the cluster in Eq. (7) can be a source and drain simultaneously when we take

$$\mu\nu = \delta^2 - \gamma^2 = -1. \quad (22)$$

We note that $|\gamma| > 1$ is the necessary condition for the existence of the spectral singularity. For the simplest case with $|\gamma| = 1$ and $\delta = 0$, the system reduces to the one which has been systematically studied in Ref. [33].

To demonstrate this point, we perform numerical simulations for the scattering center in Eq. (7) with several typical situations. First of all, the wave functions in Eq. (21) show that the state $|\alpha\rangle + i\nu|\beta\rangle$ should trigger a self-sustained emission of two counter propagating

waves; while the state $|\alpha\rangle - i\nu|\beta\rangle$ should damp as time evolution since it cannot stimulate waves from both the left and the right of infinity. Obviously, any linear superposition of above two states still can be a seed state to generate two waves prorogating to the left and the right of infinity. Similarly, any pair of state $i^j| -j\rangle + \nu i^{(j+1)}|j\rangle$ and $i^{-j}| -j\rangle + \nu i^{-(j+1)}|j\rangle$ ($j > 0$) have the same dynamical property, i.e., the former can be a seed of persistent waves; while the later should be absorbed partially by the center. In Fig. 4(a,b), we stimulate the time evolution $|\varphi(t)\rangle = e^{-iHt}|\varphi(0)\rangle$ of the initial states

$$|\varphi(0)\rangle = |\alpha\rangle + i\nu|\beta\rangle \quad (23)$$

and

$$|\varphi(0)\rangle = |\alpha\rangle - i\nu|\beta\rangle. \quad (24)$$

We see that the wave packet dynamics exhibits distinct spectral-singularity characteristics. In Fig. 4(a), state $|\alpha\rangle + i\nu|\beta\rangle$ stimulates two counter propagating waves with the amplitude ratio for the left side to right side as $1 : \nu$; while (b) state $|\alpha\rangle - i\nu|\beta\rangle$ spreads out as a short-lived seed state. It indicates that these two local states (non-orthogonal states in the framework of Dirac inner product) show total different behavior, which may be exploited to the scheme for detecting a specific state.

Secondly, any asymptotic plane-wave solution can be demonstrated by the dynamics of wavepacket. There are two typical solutions: (i) Consider a general single-incident solution, which has the form

$$(e^{-ikj} + r_k e^{ikj})| -j\rangle + t_k e^{ik(j+1)}|j\rangle \quad (25)$$

with $1 < j \leq N$. The reflection and transmission go to infinity for $k = \pi/2$. This solution corresponds to the wave emission dynamics of the initial state

$$|\varphi(0)\rangle = |\phi(N_A, \pi/2)\rangle, \quad (26)$$

The infinity of r_k and t_k should exhibit in the dynamics of the wave packet. (ii) The solution $f^{\pi/2}(j)$ corresponds to the dynamics of two counter propagating wave packets initially centered at $\pm N_A$

$$|\varphi(0)\rangle = |\phi(-N_A, k_0)\rangle - i\nu|\phi(N_A, -k_0)\rangle, \quad (27)$$

which is anti-symmetric with respect to the scattering center. The profiles of the Dirac norm of evolved states $|\varphi(t)\rangle$, i.e., $p(j, t) = |\langle j|\varphi(t)\rangle|^2$, which is the probability of the state $|\varphi(t)\rangle$ on the site j , computed by exact numerical diagonalization, are plotted in Figs. 4(c,d).

In Fig. 4(c) an incident wave packet stimulates two counter propagating emission waves with the amplitude ratio $1 : \nu$. The Dirac probabilities of reflected and transmitted waves increase linearly as time goes on, which is a dynamical demonstration of the infinite reflection and transmission coefficients. In Fig. 4(d), a typical example of complete absorption is shown. Two incident waves with matching amplitudes and relative phases are fully absorbed after scattering.

In fact, all the simulation results can be understood by an equivalent model. We introduce the transformation

$$\overline{|j\rangle} = \begin{cases} \sqrt{\nu/\mu} |j\rangle, & (j \geq 1, j = \beta) \\ |j\rangle, & (j \leq 1, j = \alpha) \end{cases}, \quad (28)$$

and its conjugation

$$\overline{\langle j|} = \begin{cases} \sqrt{\mu/\nu} \langle j|, & (j \geq 1, j = \beta) \\ \langle j|, & (j \leq 1, j = \alpha) \end{cases}, \quad (29)$$

which satisfy the biorthonormal relation

$$\overline{\langle j|l\rangle} = \delta_{jl}. \quad (30)$$

One can rewrite the Hamiltonian H_{eq} as

$$\begin{aligned} h_{\text{eq}} = & - \sum_{j=1}^{\infty} \left(\overline{|j\rangle\langle j+1|} + \overline{|-j\rangle\langle -j-1|} \right) \\ & - \left(\overline{|-1\rangle\langle \alpha|} + \overline{|1\rangle\langle \beta|} \right) + \text{H.c.} \\ & - \sqrt{\mu\nu} \overline{|\alpha\rangle\langle \beta|} - \sqrt{\mu\nu} \overline{|\beta\rangle\langle \alpha|}, \end{aligned} \quad (31)$$

which becomes Hermitian in the case of $\mu\nu > 0$. We would like to point out that the above transformation is suitable for all range of parameters (μ, ν) [49]. In the case of $\mu\nu = -1$, although it is non-Hermitian, it has \mathcal{P} symmetry, which allows us to block-diagonalize the matrix. It is shown that (see Appendix b) h_{eq} can be decomposed to two independent sub-Hamiltonians, which represent semi-infinite chains with ending imaginary potential i and $-i$, respectively. According to Refs. [48, 50], each sub-Hamiltonian has its own spectral singularity. It provides a clear physical picture for understanding the coexistence of two spectral singularities in the original system H at the point $\gamma^2 - \delta^2 = 1$.

VI. ABSORPTION OF INCOHERENT WAVE

We would like to address that the k -independent reflectionless transmission is unconditional. It is based on the fact that the equivalent Hamiltonian Eq. (17) is applicable for an arbitrary state, including a mixed state. On the other hand, in the limit case $\nu \rightarrow 0$, or $\gamma - \delta \ll \delta^2 - \gamma^2 = 1$, the transmitted probability is attenuated to nothing. In this sense, the non-Hermitian scattering center acts as a perfect absorber. Note that by combining two above features, we find that it presents an incoherent perfect absorption.

In order to clearly demonstrate this point, we consider the system with the modified lead Hamiltonian

$$H_{\text{lead}} = - \sum_{j=1}^{\infty} |j\rangle\langle j+1| - \sum_{j=N_0}^{\infty} |-j\rangle\langle -j-1| + \text{H.c.} \quad (32)$$

We take an open boundary condition at N_0 -site, in order to avoid the particle probability escaping to the left. We

examine the function of the scattering center by calculating the time evolution of a given mixed state located in the region $[-N_0, -1]$. Intuitively, any local state near the one end of the semi-infinite uniform chain should spread out to the right infinitely. In principle, it is due to the absence of bound state in a semi-infinite uniform chain.

In general, a mixed state is described by a density matrix $\rho(t)$, which obeys the Schrödinger equation

$$i \frac{\partial \rho(t)}{\partial t} = [H, \rho(t)]. \quad (33)$$

The solution of the equation has the form

$$\rho(t) = e^{-iHt} \rho(0) e^{iH^\dagger t}, \quad (34)$$

which is basis for numerical simulation in the following. The Dirac probability at j -th site can be obtained as

$$p(j, t) = \text{Tr}[|j\rangle\langle j| \rho(t)], \quad (35)$$

where $\text{Tr}[\dots]$ denotes the trace of a matrix. Then the total probability at time t is

$$P(t) = \sum_{j=-N_0}^{\infty} p(j, t). \quad (36)$$

We consider the time evolution of an initial mixed state density matrix

$$\rho(0) = \frac{1}{N_0} \sum_{j=1}^{N_0} |-j\rangle\langle -j|, \quad (37)$$

under several typical parameters $\{\gamma, \delta\}$ satisfying $\delta^2 - \gamma^2 = 1$. Fig. 6 presents the plots of the numerical results. It indicates that the probability in the whole system drops rapidly within a certain period of time, and optimal parameters can lead to near perfect absorption. State $\rho(0)$ contains components that cover all possible k . Although we cannot give a proof, our calculation indicates that such an absorber can be used to treat all kind of states.

VII. SUMMARY

In summary, we have studied the non-Hermitian Aharonov-Bohm interferometer. We have shown that the combination of imaginary potentials and magnetic flux can result in asymmetric transmission, which is not achievable in principle when one of them is solely present, which is not achievable when either one is solely present. Inspired by this, we construct an equivalent non-Hermitian dimer with an unequal hopping rate, which as a fundamental non-Hermitian element has been shown to have many intriguing features, by an interferometer-like cluster in the framework of tight-binding model. It is the first time to establish an exact equivalence between

two non-Hermitian building blocks, which paves the way for the non-Hermitian device design. As an application, this configuration can act as a unidirectional quantum amplifier. The remarkable feature of this design is wave-vector independent, which allows the reflectionless amplified transmission of a signal without any distortion. Furthermore, with optimal system parameters, it acts as an absorber for both coherent and incoherent incident waves, which may be applicable to photovoltaic or stealth technology. In addition, we investigate the dynamical behaviors related to the spectral singularities analytically and numerically.

Appendix: a. On-site potential scattering

We consider a general scattering center, an on-site potential V which may be real or complex, embedded in the center of an infinite chain with the Hamiltonian

$$H_V = H_{\text{lead}} + H_c \quad (\text{A.1})$$

where

$$H_{\text{lead}} = - \sum_{j=1}^{\infty} (|j\rangle \langle j+1| + |-j\rangle \langle -j-1| + \text{H.c.}), \quad (\text{A.2})$$

is the Hamiltonian of two leads and the scattering center Hamiltonian

$$H_c = -(|-1\rangle + |1\rangle) \langle 0| + \text{H.c.} + V |0\rangle \langle 0|. \quad (\text{A.3})$$

The Bethe Ansatz solution has the form

$$(e^{-ikj} + r_k e^{ikj}) |-j\rangle + t_k e^{ik(j+1)} |j\rangle, \quad (j > 0) \quad (\text{A.4})$$

By solving the Schrödinger equation [29], the transmission and reflection amplitudes are obtained as

$$t_k = \frac{2i \sin k}{2i \sin k - V}, \quad r_k = \frac{V}{2i \sin k - V}. \quad (\text{A.5})$$

For real V , the transmission and reflection coefficients $T_k = |t_k|^2$, $R_k = |r_k|^2$ are expressed as

$$T_k = \frac{4 \sin^2 k}{4 \sin^2 k + V^2}, \quad R_k = \frac{V^2}{4 \sin^2 k + V^2}, \quad (\text{A.6})$$

while an imaginary potential $V = i\gamma$ leads to

$$T_k = \frac{4 \sin^2 k}{(2 \sin k - \gamma)^2}, \quad R_k = \frac{\gamma^2}{(2 \sin k - \gamma)^2}. \quad (\text{A.7})$$

Appendix: b. Double spectral singularities

The Hamiltonian H has double spectral singularities, which can be understood from following derivation. Introducing a linear transformation

$$\begin{aligned} \overline{|-l\rangle} &= \frac{1}{\sqrt{2}} (|\overline{j}\rangle + \overline{|-j\rangle}), \quad \underline{|-l\rangle} = \frac{1}{\sqrt{2}} (|\overline{j}\rangle - \overline{|-j\rangle}), \\ \overline{|0\rangle} &= \frac{1}{\sqrt{2}} (|\overline{\alpha}\rangle + \overline{|\beta\rangle}), \quad \underline{|0\rangle} = \frac{1}{\sqrt{2}} (|\overline{\alpha}\rangle - \overline{|\beta\rangle}), \end{aligned} \quad (\text{A.1})$$

we have

$$h_{\text{eq}} = h_+ + h_-, \quad (\text{A.2})$$

where

$$h_+ = - \sum_{l=1}^{\infty} (\overline{|-l\rangle} \langle -l-1| + \text{H.c.}) + i \overline{|0\rangle} \langle 0|, \quad (\text{A.3})$$

and

$$h_- = - \sum_{l=1}^{\infty} (\underline{|-l\rangle} \langle -l-1| + \text{H.c.}) - i \underline{|0\rangle} \langle 0|. \quad (\text{A.4})$$

It is easy to check that

$$[h_+, h_-] = 0. \quad (\text{A.5})$$

The physical picture is clear that h_{eq} can be decomposed to two independent sub-Hamiltonian h_{\pm} , which represents semi-infinite chain with an ending imaginary potential $\pm i$. Each sub-Hamiltonian has its own spectral singularity. It is essential for the double spectral singularities in the original system H at the point $\gamma^2 - \delta^2 = 1$.

Accordingly, the dynamical behavior of spectral singularities for h_{\pm} can be demonstrated by the time evolutions of following typical initial states. (i) Position state $\overline{|0\rangle}$, which corresponds to state in Eq. (23). (ii) Position state $\underline{|0\rangle}$, which corresponds to state in Eq. (24). (ii) Gaussian wave packet $\Omega_0^{-1/2} \sum_{j < -1} e^{-\frac{\lambda^2}{2}(j-N_A)^2} e^{ik_0 j} \underline{|j\rangle}$, which corresponds to state in Eq. (26).

ACKNOWLEDGMENTS

We acknowledge the support of the National Basic Research Program (973 Program) of China under Grant No. 2012CB921900, CNSF (Grant No. 11374163), NSFC (Grant No. 11605094) and the Baiqing Plan of Nankai University.

-
- [1] C. M. Bender and S. Boettcher, Phys. Rev. Lett. **80**, 5243 (1998); C. M. Bender, D. C. Brody, and H. F. Jones, Phys. Rev. Lett. **89**, 270401 (2002).
 - [2] P. Dorey, C. Dunning, and R. Tateo, J. Phys. A **34**, 5679 (2001).
 - [3] A. Mostafazadeh, J. Math. Phys. **43**, 205 (2002); A. Mostafazadeh and A. Batal, J. Phys. A **36**, 7081 (2003).
 - [4] M. Znojil, Phys. Lett. A **259**, 220-223 (1999); Phys. Lett. A **285**, 7-10 (2001).
 - [5] H. F. Jones, J. Phys. A **38**, 1741 (2005); Phys. Rev. D **76**, 125003 (2007).
 - [6] R. El-Ganainy, K. G. Makris, D. N. Christodoulides, and Z. H. Musslimani, Opt. Lett. **32**, 2632-2634 (2007).
 - [7] Z. H. Musslimani, K. G. Makris, R. El-Ganainy, and D. N. Christodoulides, Phys. Rev. Lett. **100**, 030402 (2008).
 - [8] K. G. Makris, R. El-Ganainy, D. N. Christodoulides, and Z. H. Musslimani, Phys. Rev. Lett. **100**, 103904 (2008).
 - [9] Y. N. Joglekar, D. Scott, M. Babbey, and A. Saxena, Phys. Rev. A **82**, 030103(R) (2010).
 - [10] D. D. Scott and Y. N. Joglekar, Phys. Rev. A **83**, 050102(R) (2011).
 - [11] Y. D. Chong, L. Ge, H. Cao, and A. D. Stone, Phys. Rev. Lett. **105**, 053901 (2010); Y. D. Chong, L. Ge, and A. D. Stone, Phys. Rev. Lett. **106**, 093902 (2011).
 - [12] H. Jing, S. K. Özdemir, Xin-You Lü, J. Zhang, L. Yang, and F. Nori, Phys. Rev. Lett. **113**, 053604 (2014).
 - [13] A. Guo, Phys. Rev. Lett. **103**, 093902 (2009).
 - [14] C. E. Rüter, et al. Nat. Phys. **6**, 192-195 (2010).
 - [15] W. Wan, Y. Chong, L. Ge, H. Noh, A. D. Stone, and H. Cao, Science **331**, 889-892 (2011).
 - [16] Y. Sun, W. Tan, H.-Q. Li, J. Li, and H. Chen, Phys. Rev. Lett. **112**, 143903 (2014).
 - [17] L. Feng, et al. Nature Mater. **12**, 108-113 (2013).
 - [18] B. Peng, et al. Nat. Phys. **10**, 394-398 (2014).
 - [19] L. Chang, et al. Nature Photon. **8**, 524-529 (2014).
 - [20] L. Feng, Z. J. Wong, R.-M. Ma, Y. Wang, and X. Zhang, Science **346**, 972-975 (2014).
 - [21] H. Hodaei, et al. Science **346**, 975-978 (2014).
 - [22] M. Wimmer, et al. Nat. Commun **6**, 7782 (2015).
 - [23] J. G. Muga, J. P. Palaob, B. Navarro, and I. L. Egusquiza, Phys. Rep. **395**, 357 (2004).
 - [24] F. Cannata, J-P. Dedonder, and A. Ventura, Ann. Phys. **322**, 397 (2007).
 - [25] X. Q. Li, X. Z. Zhang, G. Zhang, and Z. Song, Phys. Rev. A **91**, 032101 (2015).
 - [26] Z. Ahmed, Phys. Lett. A **377**, 957-959 (2013).
 - [27] A. Mostafazadeh, J. Phys. A: Math. Theor. **47**, 505303 (2014);
 - [28] S. Longhi, Opt. Lett. **40**, 1278-1281 (2015).
 - [29] W. Kim, L. Covaci, and F. Marsiglio, Phys. Rev. B **74**, 205120 (2006).
 - [30] S. Yang, Z. Song, and C. P. Sun, Phys. Rev. A **73**, 022317 (2006).
 - [31] L. Jin and Z. Song, Phys. Rev. A **81**, 032109 (2010).
 - [32] L. Jin and Z. Song, Phys. Rev. A **80**, 052107 (2009).
 - [33] G. Zhang, X. Q. Li, X. Z. Zhang, and Z. Song, Phys. Rev. A **91**, 012116 (2015).
 - [34] Qi-Bo Zeng, S. Chen, and R. Lü, arXiv: 1608.00065 (2016).
 - [35] N. Hatano and D. R. Nelson, Phys. Rev. Lett. **77**, 570 (1996); Phys. Rev. B **56**, 8651 (1997).
 - [36] A. Mostafazadeh, Phys. Rev. A **80**, 032711 (2009).
 - [37] S. Longhi, Phys. Rev. B **80**, 165125 (2009).
 - [38] A. Mostafazadeh, Phys. Rev. Lett. **110**, 260402 (2013).
 - [39] A. Mostafazadeh, Phys. Rev. A **84**, 023809 (2011).
 - [40] A. A. Andrianov, F. Cannata, and A. V. Sokolov, J. Math. Phys. **51**, 052104 (2010).
 - [41] F. Correa and M. S. Plyushchay, Phys. Rev. D **86**, 085028 (2012).
 - [42] A. Mostafazadeh and M. Sarisaman, Phys. Rev. A **87**, 063834 (2013).
 - [43] L. Chaos-Cador and G. Garcia-Calderon Phys. Rev. A **87**, 042114 (2013).
 - [44] A. Mostafazadeh and M. Sarisaman, Phys. Rev. A **88**, 033810 (2013).
 - [45] M. Fagotti, C. Bonati, D. Logoteta, P. Marconcini, and M. Macucci, Phys. Rev. B **83**, 241406(R) (2011).
 - [46] K. Ding, Z. Q. Zhang, and C. T. Chan, Phys. Rev. B **92**, 235310 (2015).
 - [47] A. Mostafazadeh, Phys. Rev. Lett. **102**, 220402 (2009).
 - [48] X. Z. Zhang, L. Jin, and Z. Song, Phys. Rev. A **87**, 042118 (2013).
 - [49] X. Z. Zhang and Z. Song, Ann. Phys. **339**, 109 (2013).
 - [50] S. Longhi, Phys. Rev. B **80**, 165125 (2009).